



# Design optimization of giant magneto resistance–based magnetic nanoparticle detection in liquid samples for biomedical applications

G. Anand · T. Thyagarajan · D. Kokila · C. Kamal

Received: 6 September 2021 / Accepted: 3 May 2022  
© The Author(s), under exclusive licence to Springer Nature B.V. 2022

**Abstract** In this paper, the design of a Giant Magneto Resistive (GMR) sensor is optimized using single-objective optimization algorithms, for measuring magnetic nanoparticles stored in an Eppendorf tube. The iron oxide nanoparticle ( $\text{Fe}_3\text{O}_4$ ) is employed as a magnetic nanoparticle. The variance-based sensitivity analysis is used to identify the most significant variable affecting the GMR sensitivity which is found to be the magnetic bias. As a result, using single-objective optimization algorithms, the optimal value for GMR sensor magnetic bias value ( $H$ ) was computed and incorporated in the instrument design. The device thus designed was fabricated using Rapid Prototyping (RPT)-solid works. To identify the sensor response in a linear range, a couple of permanent neodymium magnets were used to provide horizontal and vertical magnetic fields for sensor bias and nanoparticle magnetization. This process gives an idea of a combined hardware-software approach, to reduce the measurement uncertainty and increase the system's sensitivity. The proposed design achieved an output signal change of 248 mV for a magnetic particle concentration change of 1  $\mu\text{g}$ . The device's lowest measurable

concentration was improved using the appropriate single-objective optimization technique, resulting in 36 ng as the lowest measurable concentration. The performance of the optimal GMR device design was analyzed for hysteresis analysis  $\text{Fe}_3\text{O}_4$ , Distance vs Sensor output for various input voltages, Temperature performance and SEM analysis of  $\text{Fe}_3\text{O}_4$ . The average nanoparticle size range is measured as 97 nm from SEM analysis.

**Keywords** Biomedical · Ferromagnetism · GMR sensor · Single objective optimization · Magnetic nanoparticles

## Introduction

Magnetic nanoparticles are employed in a variety of applications in healthcare, including biological identification and quantification, biomolecule separation, cell identification, medication administration, and bio probes. Bio probes bind a magnetic nanoparticle (MNP) to a target agent via a biological process, which is subsequently measured by magnetic field sensors for medical diagnostics. Nanoparticles are used in conjunction with electrical or electrochemical sensing in many biomedical applications. Giant Magneto Resistance (GMR) sensor–based Magnetic Nano Particles (MNPs) detection is an interdisciplinary approach combining sensitive biosensors and magnetic resistance principles for the biological agents.

**Supplementary Information** The online version contains supplementary material available at <https://doi.org/10.1007/s11051-022-05484-6>.

G. Anand (✉) · T. Thyagarajan · D. Kokila · C. Kamal  
Department of Instrumentation Engineering, Madras  
Institute of Technology, Anna University, Chennai, India  
e-mail: g.anand777@annauniv.edu.in

The premise behind Giant Magnetic Resistance GMR detection (Atalay et al. 2018) is that a stray field from MNPs bound on the surface of biological agents in a liquid sample can affect the magnetization in the free layer, causing a change in resistance in the GMR sensor. The GMR sensor is made up of many layers, with magnetic (ferromagnetic) and non-magnetic layers alternating in the multilayer (conductive) (Li et al. 2013). It is also possible to use a magnetic field to alter electrical resistance on the nanoscale (Muşuroi et al. 2021).

The magnetic field moments of the ferromagnetic layers are side-by-side in structure (Reig et al. 2009). If the magnetic field moment of the ferromagnetic layer is anti-parallel, the corresponding spin dispersion will be substantial and the resistance value of the material will be high. GMR sensors are used to monitor the intensity of the magnetic field in a variety of applications (Reig et al. 2009).

Chip-based GMR spin valves, in combination with MNPs (Li et al. 2010), have evolved into an effective instrument for high sensitivity, real-time electrical readout and efficient biomolecule detection.

Magnetically tagged biomolecules may be detected quantitatively using giant magnetoresistive biosensors in biomedical applications (Li et al. 2010). Biological and biomolecular agents such as viruses, proteins, bacteria and nucleic acids are detected using GMR technology in biosensors (Sun et al. 2018). Furthermore, for immunoassay applications, GMR chips may be combined with not just electronics but also with microfluidics (Crespo et al. 2018). MNPs do not fade, unlike fluorescent markers employed in immunofluorescence procedures (Park 2016). Also, biological samples lack the ferromagnetism feature, enabling the detection of magnetic signals with reduced background noise (Manteca et al. 2011).

One of the most valuable tools of artificial intelligence is single objective optimization algorithms (SOOAs). To identify the lowest sample concentration, the optimal design of GMR for MNP detection has been developed using SOOA with efficiency, high sensitivity, high performance and repeatability as the objective functions.

SOOA techniques (Chakkarapani et al. 2018) namely: Genetic algorithm (GA), Partial Swarm optimization (PSO) algorithm, Firefly (FF) algorithm, and Ant Colony Optimization (ACO) are employed for the design optimization and analysis of GMR-based MNP detection. Various design parameters influence the performance of the GMR-based MNP detection such as magnetic biasing of the sensor, Magnetic field orientation of the sensor and biasing magnet and distance between sample and GMR sensor (Park 2015). The selection of design parameters is a crucial part of process optimization.

The most influencing design parameter for GMR-based MNP detection is determined by performing sensitivity analysis. The optimization of various parameters is scalarized into a single objective function (magnetic bias) using a variance-based sensitivity index. The schematic diagram of the GMR sensor and the corresponding basic integrated circuit (IC) structure is shown in Fig. 1. The pinned layer and a free layer make up the fundamental GMR material structure; An external magnetic field in the linear range of 10 to 70 Oe can impact the free layer. In a cosine relationship, the angle between the free layer and the pinned layer impacts the sensor's output.

Identifying appropriate SOOA that results in better performance and sensitivity with minimal sample concentration, and embedded firmware development for nanoparticle identification from GMR signals are the novel aspects of our research.

**Fig. 1** Functional block diagram of GMR

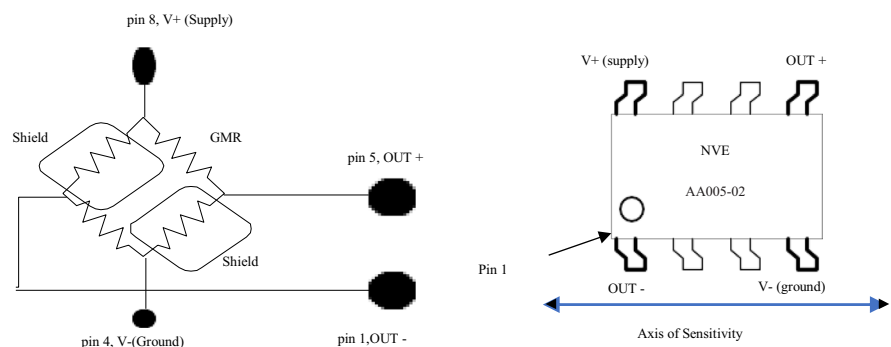


**Table 1** Sensor specifications

Sensor		AA005-02
Liner range	Min	10 (Oe)
	Max	70 (Oe)
Saturation		100 (Oe)
Sensitivity	Min	0.45 (mV/V-Oe)
	Max	0.65 (mV/V-Oe)
Max-Non-Linearity		2%
Max. Hysteresis		4%
Max Operating Temp		125°C
Typ. Resistance		5kΩ
Package		SOIC8

**Materials and methods**

The specifications of GMR sensor AA005-02 are presented in Table 1. These sensors are distinguished by their high sensitivity to the applied magnetic fields, better temperature stability, low power consumption, and small size. They are appropriate for use in hand-held instruments and implanted medical devices because of these features (Manteca et al. 2011). These simple magnetic sensors are a good choice for a wide range of analog sensing applications due to their unrivaled adaptability (Murzin et al. 2020).

The sensitivity of these sensors is cosine-scaled as the sensor is rotated away from the sensitive direction in the plane of the IC. Furthermore, regardless of whether magnetic fields are positive or negative along the sensitivity axis, these devices provide the same output (Omni polar output). With a 5 V power supply, the highest signal output from the sensor element is approximately 350 mV at 100 Gauss.

Iron (II, III) oxide, nano powder and molecular weight of 231.54 g/mol (CAS Number: 1317–61-9) from Thermo Fisher Scientific™ (Alfa Aesar) are insoluble in water and organic solvents. They are soluble in concentrated mineral acids. The specifications of nanoparticles are presented in Table 2. The need for magnetic nanoparticles, based on literature (Laha 2015) and commercial availability Fe<sub>3</sub>O<sub>4</sub> is chosen in this research work.

**Mathematical modelling of GMR**

As stated by the general Eq. (1), the basic assumption of Magneto Resistance (MR) is the

**Table 2** Specification of nanoparticles

Specifications	
Physical form	50–100 nm APS powder
Particle size	30 to 50 nm APS
Surface area	20 to 50 m <sup>2</sup> /g
Density	5.2 g/mL
Melting point	1538 °C
Purity	99.50%

modification of a material’s resistivity as a response to an external magnetic field:

$$R = f(B) \tag{1}$$

The Lorentz force on electrons, which is described in Eq. (2) is originated from semiclassical considerations as normal magnetoresistance.

$$\vec{F} = m \left( \frac{d\vec{v}}{dt} \right) = e\vec{E} + (e\vec{v} \times \vec{B}) \tag{2}$$

and the current density is given in Eq. (3)

$$\vec{j} = \left( \frac{ne^2\tau}{m} \right) \vec{E} + \left( \frac{e^2\tau}{m} \right) \vec{v} \times \vec{B} \tag{3}$$

where  $\vec{v}$  = Electron velocity,  $\vec{F}$  = Lorentz force,  $\vec{E}$  = Electric field,  $\tau$  = Relaxation time,  $\vec{B}$  = Magnetic field,  $\vec{j}$  = Current density, n = Electron concentration, m = Electron mass and e = Electron charge.

The Lorentz force is the source of the Hall effect. The magnetic field causes the current path to deviate, increasing the current path length and as a result, an increase in the effective resistance, as stated in Eq. (4) (Reig et al. 2009).

$$R = R_0 \frac{\rho_B}{\rho_0} (1 + C_1 (\mu B^2)) \tag{4}$$

where  $\rho_B/\rho_0$  = specific relative resistance,  $R_0$  = resistance at the null field, and  $C_1$  = geometrical parameter. The low MR level significantly limits the application of this concept in magnetic sensing.

The difference in the functional behaviour of change of the magnetic field  $B_x$  experienced by a pair of resistors  $R_1, R_3$  and  $R_2, R_4$  is the source of sensor output voltage as a function of vertical distance dz. (Behera, et al. 2021). The Eq. (5) is used to calculate the theoretical output voltage from an

ideal GMR sensor response at  $dx = 1$  mm (Behera, et al. 2021)

$$V_{out}(d_z) = V_{in} \left( \left( \frac{R_4}{R_1 + R_4} \right) - \left( \frac{R_3}{R_2 + R_3} \right) \right) \quad (5)$$

When an external magnetic field is applied, a GMR-based magnetic sensor operates by measuring the effect of a large change in the resistance of a metal. The value of the magnetoresistance (MR) ratio is given in Eq. (6) (Djamal and Ramli 2017)

$$MR = \frac{\Delta R}{R} = \frac{R(H) - R(H = 0)}{R(H = 0)} \quad (6)$$

$R(H=0)$  is the resistance of the device when no external magnetic field is applied,  $H$  is the magnetic field strength and  $R(H)$  is the resistance of the device when it is influenced by an external magnetic field.

### Signal conditioning

The usefulness of NVE corporation's sensors is increased by adding signal processing circuits to the basic sensor unit. Compared to sensors that require more amplification to generate a useable output, the GMR sensor element has a larger output signal, which implies less circuitry, lower signal errors, less drift and greater temperature stability. Due to their high signal strength, rapid reaction under a lower magnetic field, small size, high sensitivity, frequency responsiveness, decreased power consumption and low cost, GMR sensors have become a major player in the field of magnetic sensing ((Daughton 2000; Smith and Schneider 1998)). These benefits of GMR sensors are counterbalanced by a drawback that makes it difficult to evaluate the accuracy of the output reading. The output obtained will be feeble (Zhang et al. 2016). To address this flaw, an advanced signal conditioning circuit needs to be designed.

The signal conditioning unit converts the electrical signal to the anticipated voltage level (Bhaskar-rao et al. 2017). Due to numerous factors such as electrical or radio frequency noise, cable loss and so on, many sensors do not produce a clean and clear signal (Elangovan and Anoop 2020). Before being recorded and processed by a data collection device, such signals must pass through a signal conditioning unit. Amplification, isolation, filtering, coupling and

**Table 3** Total harmonic distortion

For 50 Hz	SNR (dB)	CMRR (dB)
Band stop filter	19.5	-63
Band reject filter	42	-65
Notch filter	6	-67.5

**Table 4** Power dissipation

Instrumentation amplifier	Power dissipation (mW)
OP07	227
AD822	162
INA118	90

linearization are just a few of the numerous processes that go into signal conditioning.

Three filter circuits namely: Band Stop Filter, Band Reject Filter and Notch Filter are designed. Their performance is compared by considering the Signal to Noise Ratio (SNR), Common Mode Rejection Ratio (CMRR) and the Total Harmonic Distortion (THD) as presented in Table 3 and accordingly, Notch filter is selected (Anand et al. 2022).

For signal enhancement, the Instrumentation amplifiers namely OP07, AD822, INA118 are employed. Based on the comparison of power dissipation, as given in Table 4, the desired instrumentation amplifier namely, INA118 is selected. The alternating coupling permits only AC signals to pass through a connection and it removes the DC offset and vice versa for the direct coupling circuit.

The output from the GMR sensor is very feeble which might be affected by the noise. Hence, there is a need for an appropriate signal conditioning circuit to be included in the hardware set-up to obtain better output. Based on various simulation studies for noise filtering, AC & DC coupling and amplification, the desired signal conditioning circuit is identified as shown in Fig. 2(a). The output obtained from the signal conditioning circuit is shown in Fig. 2(b).

### Design optimization of GMR sensor

The structural design optimization of the GMR sensor is obtained by making use of SOOA. The major

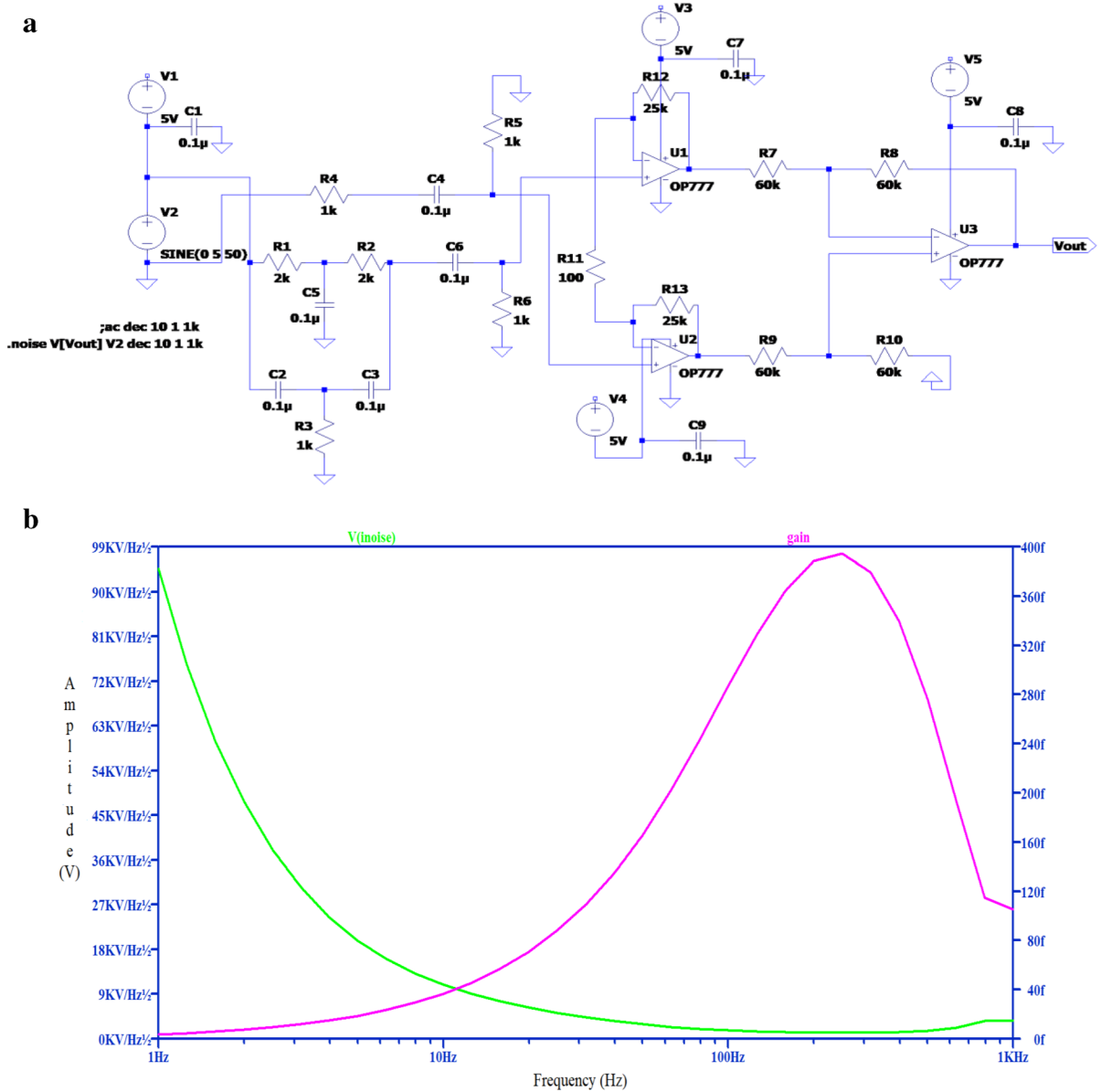


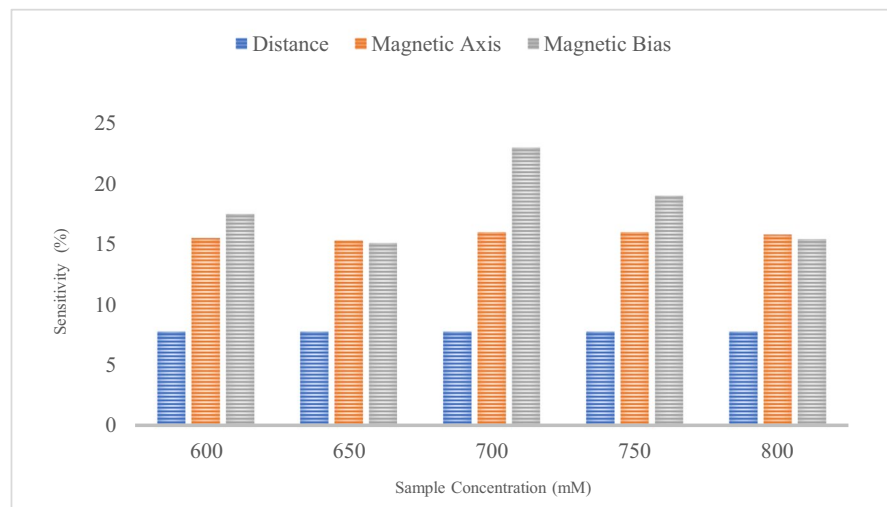
**Fig. 2** (a) Signal conditioning circuit, (b) Signal conditioning output

design variable that influences the performance measure of the GMR sensor is chosen, based on the sensitivity analysis (Lee et al. 2014). The GMR sensor has many design factors namely: distance between sensor, magnet, and sample (D), magnetic bias (H), magnetic axis. Any change in these design variables might impact the sensor’s performance. Sensitivity analysis is performed to identify the most significant design variable that affects the GMR sensor’s performance.

The following steps are involved in sensitivity analysis: Definitive screening design, Variance-based sensitivity analysis, Main effect, Total Effect, Screening of design variables. Based on the variance-based sensitivity indices and sensitivity indices of concentration range measurement to 3 variables, magnetic bias is considered as an optimization variable as Fig. 3.

Magnetic bias and magnetization: A pair of permanent magnets (Neodymium magnets) were attached to

**Fig. 3** Comparison of sensitivity indices of concentration range measurement obtained using 3 design variables



the sides and another to the lower part of the GMR sensor, respectively (Park 2015). The induced magnetic field components magnetize the magnetic nanoparticles and bias the GMR sensor to maximize the sensitivity. As a result, permanent magnets facing each other diagonally, produce vertical and horizontal magnetic field components. The magnetic nanoparticles are magnetized and the GMR sensor is biased by the generated vertical and horizontal magnetic field components (Park 2015).

#### A Definitive screening design

By using this design, the significant components that have a considerable influence on the reaction are separated from a large number of inconsequential factors that have little effect (Chakkarapani et al. 2018). As part of the affectability research, the design screening configuration is employed.

#### B Variance based sensitivity analysis

The output sensitivity to an input variable is calculated using variance-based sensitivity, which is based on the amount of variation in the output caused by the corresponding input. Assuming that  $x_1, x_2, \dots, x_n$  are the components in the prototype, then the foresight model is represented by the function  $f$  as given in Eq. (7) (Chakkarapani et al. 2018).

$$y = f(x_1, x_2, \dots, x_n) \quad (7)$$

#### C Main effect

$\text{Var}(E(y|x_j))$  can be used to denote the influence of the main effect  $x_j$  on 'y'. For the given  $x_j$  the expectation is calculated, with conditional distribution  $x_1, x_2, x_3, \dots, x_n$ . Over the  $x_j$  distribution, the variance is determined in the mean of y. For the main effect to measure the sensitivity index  $S_i$  for  $x_j$  is given in Eq. 8 (Chakkarapani et al. 2018).

$$S_i = \frac{\text{Var}(E(y|x_j))}{\text{Var}(y)} \quad (8)$$

#### D Total effect

The total effect column represents the overall contribution to Eq. (7)'s the variance from all expressions that contain  $x_j$ . The function 'f' is split into functions that represent the effects of single variables, pairs of variables, and so on, as well as the sum of a constant. The two factors namely,  $x_1$  and  $x_2$ ; then the total effect index for  $x_1$  is an estimate of  $T_i$  which is given in Eq. (9).

$$T_i = \frac{\text{Var}(E(y|x_1)) + \text{var}(E(y|x_1, x_2))}{\text{Var}(y)} \quad (9)$$

#### E Screening of design variables

For the objective function containing concentration range measurement, the sensitivity indices of design variables namely main effect and total effect are computed using variance-based sensitivity and are presented in Table-5. Based on the sensitivity analysis presented in Table 5, it is

**Table 5** Variance-based sensitivity indices

Design variable	Main effect	Total effect
Distance (mm)	0.064	0.0813
Magnetic bias (Oe)	0.156	0.174
Magnetic axis (Oe)	0.205	0.213

found that the most significant optimization variable is magnetic bias (H).

The percentage sensitivities are also computed for the three design variables for four different concentrations and are compared as shown in Fig. 3. The comparison reveals that the magnetic bias has more sensitivity at all concentration levels.

After identifying the most significant design parameter i.e., the magnetic bias, its optimal value is computed using SOOAs namely: Genetic Algorithm (GA), Particle Swarm Optimization (PSO), Firefly (FF) algorithm and Ant Colony Optimization (ACO) algorithm employed. To perform optimization, it is required to fix the lower and upper bound for the magnetic bias. Based on the literature survey (Lee et al. 2014), the lower and upper boundary values fixed for the design variables(Magnetic bias (H)) are 20 and 30 respectively.

**A Genetic algorithm(GA)**

This algorithm is based on the principle of genetics process and natural selection. It is applied frequently to find the best possible solution or the nearest optimal solution. It consists of three major operations namely: selection, crossover, and mutation. The following are the algorithmic steps involved in GA (Chakkarapani et al. 2018).

- i The population size is set to zero. The design variable and number of objectives are fixed as one. To achieve the goals of sensitivity analysis, the most influencing variable namely magnetic bias is chosen as the design variable.
- ii Choose a population at random from the design space.
- iii Cross-over and mutation are used to create a new population.
- iv In the new population, update the design points and analyze.

**Table 6** Parameter for GA

Parameters	Value
Design variables	Magnetic bias
Size of Population	40
Generation	100
Crossover type	Single point
Parent selection	Steady-state selection
Probability of crossover	0.8
Probability of mutation	0.04

v Repeat stages (ii–iv) till the desired result is obtained.

vi Stop the optimization procedure once the intended goal is achieved.

The GA starts with a group of individuals known as the population. Every individual is a unique solution to the problem at hand. Genes are a collection of characteristics that describe an individual. To make a Chromosome (solution), genes are joined together in a string. Every individual is assigned a score and the chance of being considered for reproduction is influenced by that score. The purpose of the selection phase is to choose the best individuals and transmit their genes to the next generation. The crossover of two-parent strings produces offspring (new solutions) by swapping parts or genes of the chromosomes. During mutation operation, flipping certain genes of a string takes place to generate new solutions. Once the crossover and mutation process is completed, again the process is assessed for a new round of selection and propagation until it reaches the most appropriate solution. The parameters of GA used in the present work are listed in Table 6.

GA offers the best solution for the population and better for the tendency for premature convergence. Whereas the design variable in PSO can take any value, even outside their restrictions based on their position to calculate velocity vector. The main advantage of PSO is fast convergence compared to GA.

**B Particle Swarm Optimization algorithm (PSO)**

PSO is a stochastic optimization and nature-inspired evolutionary technique. The following is the list of the algorithmic steps involved in PSO.

- i Determine the population size. The design variable and number of objectives are set as one. To achieve the goals of sensitivity analysis goals, the most influencing variable namely magnetic bias is chosen as the design variable
- ii The fitness of each particle is evaluated
- iii Update particle positions
- iv Update individual and global best position
- v Update the particle position and velocity

$$v = v + c_1 * rand * (pBest - p) + c_2 * rand * (gBest - p) \quad (10)$$

$$p = p + v; \quad (11)$$

where  $p$  = particle's position,  $c_1$  = weight of local information, and  $c_2$  = weight of global information and  $v$  = path direction.  $gBest$  = best position of the swarm, the  $rand$  = random variable, and  $pBest$  = best position of the particle.

vi Repeat the steps (ii–iv) until the termination is satisfying.

vii End the process, after obtaining the desired convergence.

The parameters of PSO used in the present work are listed in Table 7.

The main drawback of the PSO algorithm is, it is difficult to predict the best topology in advance. Also, it is easy to fall in local optimum in high dimensional space. It has a low convergence rate in the iterative process. A better convergence rate can be achieved by Ant Colony Optimization Algorithm (ACO) compared to PSO.

### C Ant Colony Optimization (ACO)

ACO is a stochastic method for addressing computational issues that can be applied to networks to discover good paths. Multiagent techniques based on the behaviour of real ants were used by artificial ants. Initialize ACO parameters and generate the preliminary population of ACO. Assess the suitability of the ACO using the objective function. Construct solution using pheromonal path and randomization and update the amount of pheromone.

The following is a list of the algorithmic stages involved in ACO.

- i Determine the population size. The design variable and number of objectives should both be set to one. To achieve the sensitivity analysis goals, the most affected variables are chosen.
- ii Choose a population at random from the design space
- iii A selection on the shortest edges searches by pheromone updating rule
- iv The pheromone level of the edges is updated
- v Repeat the steps (ii–iv) until the termination is satisfying
- vi End the optimization process, after obtaining the desired objective is achieved

The parameters of ACO used in the present work are listed in Table 8.

If the condition is not satisfied, then the process will be performed until it gets the best solution. An optimization issue requires a single objective function, the challenge of discovering the best optimum solution. The drawback of the ACO algorithm is it is not suitable for scattering solutions. Also, it is difficult to initialize the design parameters. This can be overcome by the FF algorithm.

**Table 7** Parameter for PSO

Parameters	Value
Design variable	Magnetic bias
Size of population	40
Generation	100
$C_1$ and $C_2$	2
Inertial weight	0.98

**Table 8** Parameter for ACO

Parameters	Value
No. of objective	1
Design variable	Magnetic bias
No. of ants	40
Generation	100
$q$	0.5
Zeta	1

**D Firefly (FF) Algorithm**

The firefly optimization algorithm is a swarm-based algorithm that has different applications and popularity in a short duration. It is simple to know and execute. Different modifications are done to boost the performance of the FF algorithm. The following are the algorithmic steps involved in the FF algorithm.

- i Determine the population size. The design variable and number of objectives should both be set to one. To achieve the sensitivity analysis goals, the most affected variables are chosen.
- ii Evaluate fitness of all fireflies from the objective function
- iii Update the fitness values of fireflies
- iv Move the points in the ranking order.
- v Update the positions
- vi Repeat the steps (ii–iv) until the maximum iteration is reached.
- vii End the optimization process, after obtaining the desired convergence.

The parameters of FFO used in the present work are listed in Table 9.

Initialize FA parameters and generate the primary population of fireflies. Analyze the fitness of the fireflies using the objective function and update the light intensity. Rank the firefly and get the finest. Shift the firefly to their improved solution. The process will be repeated till it gets the best solution.

$$x_i^{t+1} = x_i^t + \beta \exp\left[-\gamma r_{ij}^2\right] \left(x_j^t - x_i^t\right) + \alpha_t \epsilon_t \quad (12)$$

**E Optimization results of GMR sensor**

**Table 9** Parameter for FFO

Parameters	Value
No. of objective	1
Design variable	Magnetic bias
Size of population	40
Generation	100
Dimension	10
Alpha	0.5
Beta	0.2
Gama	1.0

Optimal values computed from various SOOA’s namely GA, PSO, FFO, ACO are listed in Table 10. The optimal values obtained from GA, PSO, FFO, and ACO are used to design the GMR detection. The qualitative comparison of the performance of different SOOA’s is given in Table 11.

All the optimization techniques give different optimal values. From Table 11, it is observed that the GA optimization technique gives better performance in terms of execution time, memory usage, technical and procedural complexity. The optimum values obtained from all the SOOAs are used to design the GMR-based MNP detector and analyzed its performance and sensitivity in the following session.

**Experimental setup**

The block diagram of the experimental setup for the GMR-based nanoparticle detection system is shown in Fig. 4. MNPs are initially used to tag biological material (Park 2015). Bio probes are positioned near the GMR surface in a sample holder. For greater sensitivity, the GMR sensor is biased with the right gauss (35 gauss) value using neodymium magnets obtained from single-objective optimization. A 5 V DC power supply is used to power the sensor. The alignment unit is modified such that the GMR sensor and sample holder are perfectly aligned along the magnetic axis (using Solid Works and Rapid Prototyping Tool (RPT)).

Advanced signal conditioning techniques namely: enhanced filter design, high-precision amplification, and high-sensitivity magnetic biasing, have been developed in the proposed design for the accurate detection of MNPs employing GMR biosensors. The GMR sensor’s electrical signal is further processed for noise reduction and optimum amplification.

The primary source of noise is 50 Hz power line noise, which is eliminated by the notch filter. The instrumentation amplifier INA118 is used to amplify the signal.

The calibration chart is used to determine the nanoparticle detection from the signal. Embedded software

**Table 10** Comparison of optimal values

Design variable	GA	PSO	ACO	FFO
Magnetic bias (H) (Oe)	35.1	35.7	36	33.9

**Table 11** Qualitative comparison of SOOAs performance

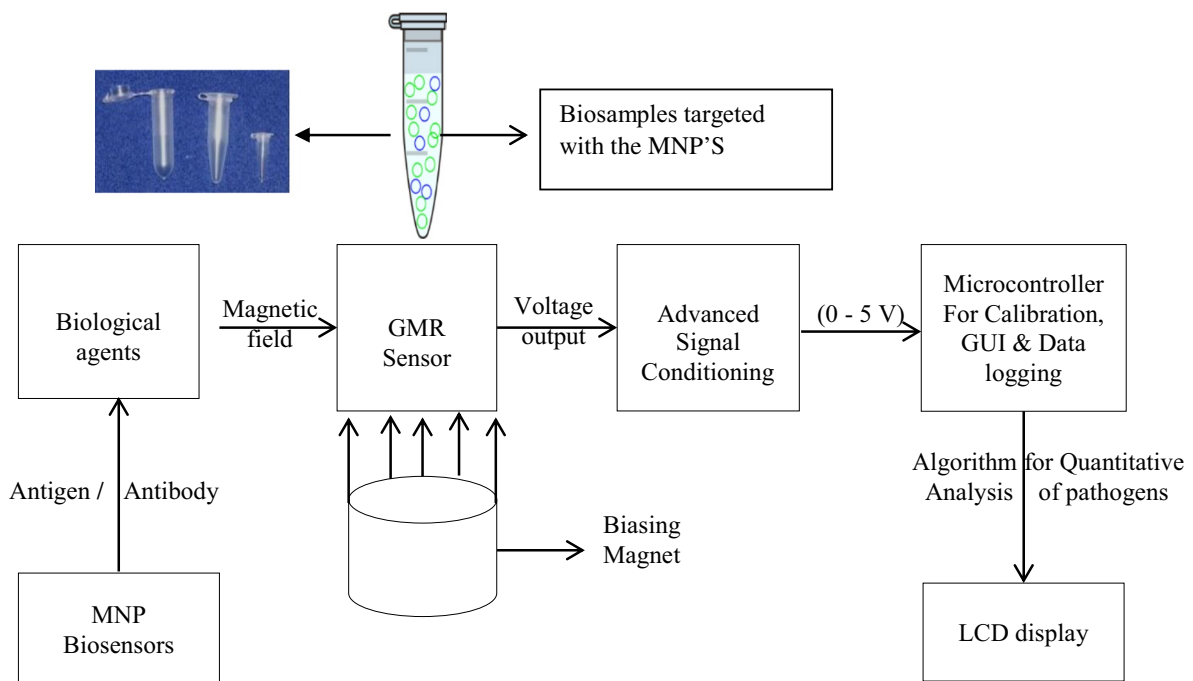
S. no	Parameter	Values obtained for SOOA			
		GA	PSO	ACO	FFO
1	Design variable	One	One	One	One
2	Execution time	Low	Low	High	Normal
3	Computational difficulty	Low	Low	High	Moderate
4	Technical complication	Simple	Average	Complex	Complex
5	Memory usage	Less	Less	High	Normal

is responsible for completing this task. The output is displayed on an LCD. Each end of the sample tube was sealed with epoxy to prevent the magnetic particles from oxidizing. Magnetic particle concentrations in the precursor solution ranged from 0  $\mu\text{g}$  to 1  $\mu\text{g}$ . Initially, the stock solution was prepared with  $\text{Fe}_3\text{O}_4$  and medical-grade ethanol. Further serial dilution was carried out as per our previous research work (Anand et al. 2021). The concentration of the stock solution was measured and verified with the help of a commercially available gauss meter – LUTRON GU-3001.

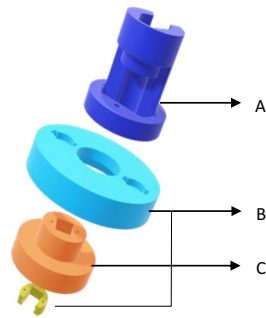
### RPT fabrication

Using Solid Works and Rapid Prototyping Tools, a unique magnetic alignment module is designed and a 3-dimensional model is developed as shown in Fig. 5 to increase sensitivity and performance. It consists of a sample holder module (A), a biasing magnet holder (B) and a sensor holder (C). Using the Lurton gauss meter, all these modules were perfectly aligned with the magnetic axis.

The three-dimensional view of the module is shown in Fig. 5. The Eppendorf with magnetic nanoparticles sample is placed in the sample holder (A).

**Fig. 4** Functional block diagram of GMR-based nano-particle detection system

**Fig. 5** 3D view of the modules



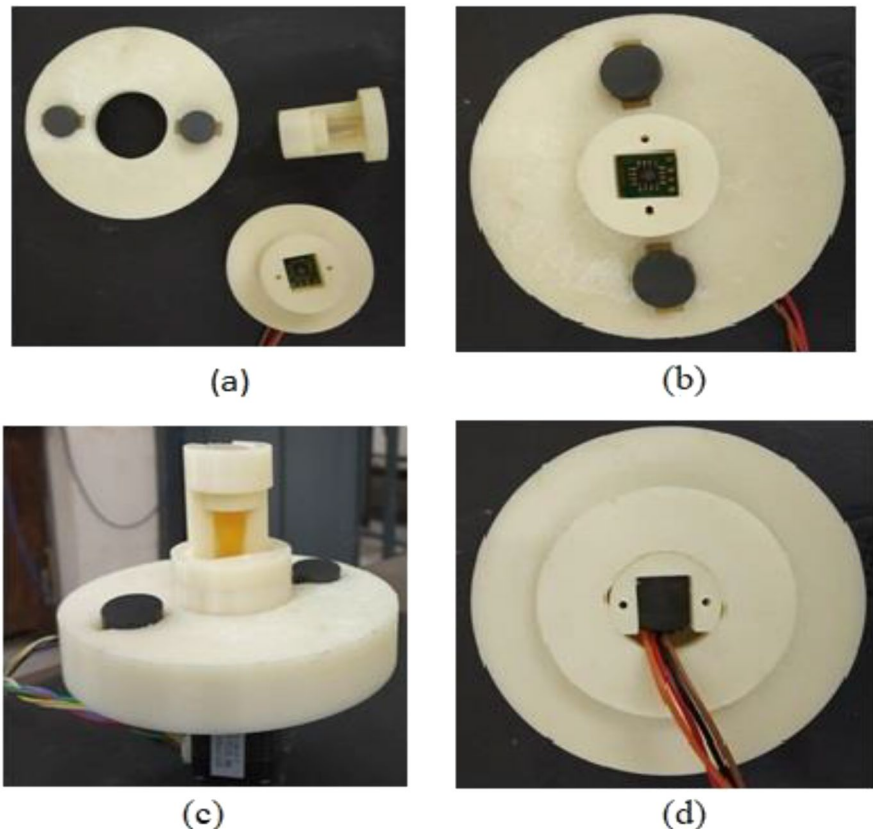
The neodymium magnets are used as the biasing magnets that magnetize the sample and are placed in the magnet holder (B) which has 360° rotation. The GMR sensor is placed in the sensor holder (C) between the magnets to measure the sample concentration. These modules were designed using a Solid works design tool and fabricated with the RPT facility.

Figure 6(a) shows the three individual components of modules designed namely: sample holder, sensor holder, and biasing magnet. Figure 6(b) gives the view of the GMR sensor placed with the biasing

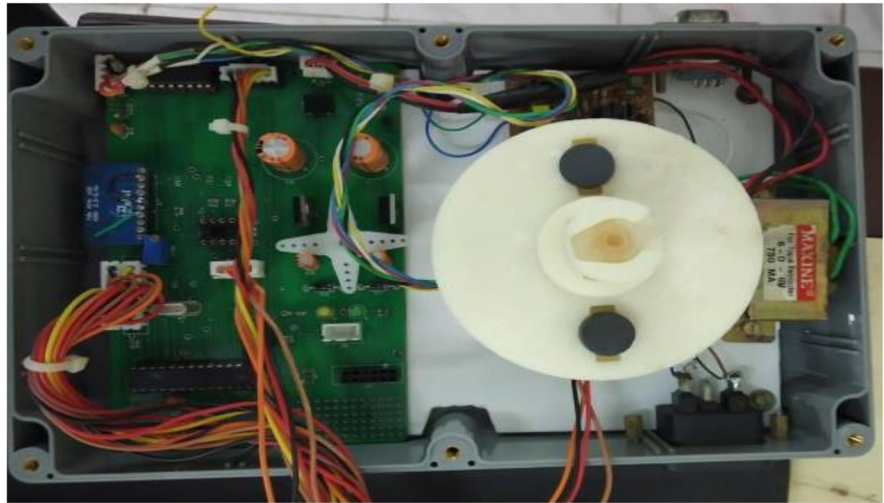
neodymium magnets. Figure 6(c) shows the placement of all three modules together. Figure 6(d) shows the bottom view of the biasing magnet.

The placement of customized Printed Circuit Board (PCB) and RPT modules inside the prototype is shown in Fig. 7. The fabricated PCB board contains analog circuits namely: filter module, instrumentation amplifier module, continuous constant power supply module, keypad control module, external Analog Digital Circuit (ADC) module, 16×2 LCD interface module and Stepper motor control (H bridge) module. The 50 Hz noise is removed with the notch filter and the signal strength of the output signal from the GMR sensor is improved with the help of the INA118 instrumentation amplifier. The stepper motor control module is used to control the magnetic biasing automatically. The Proteus simulation tool is used to design and develop analog circuits along with the microcontroller controller for a better user-friendly HMI interface. The measurement of MNPs is performed by simply pressing the keypad button which makes the proposed device much easier to operate.

**Fig. 6** Fabricated Magnetic Alignment modules using Rapid prototyping



**Fig. 7** Internal view of GMR prototype



## Result and discussion

### Scanning electron micrograph (SEM)

Figure 8 shows the SEM images for the Iron (II, III) oxide MNPs at different magnifications was carried out using Vega3 Tescan Instrument. Figure 8(a) and (b) shows the microscopic view at 500 $\times$  and 2500 $\times$  magnification. The physical characteristics of the magnetic nanoparticles such as surface morphology, topography, surface area, structure, size, shape, etc. are studied using SEM analysis. From Fig. 8(a) and (b), it is observed that the nanoparticle surface is porous, uneven and has rough surface area. The average nanoparticle size ranges by 97 nm.

The hysteresis loop (Reig et al. 2009) of Fe<sub>3</sub>O<sub>4</sub> nanoparticles revealed that the magnetic nanoparticles had a large  $M_s$  of 62 emu/g, which is similar to the  $M_s$  of bulk Fe<sub>3</sub>O<sub>4</sub> (69.5 emu/g) (Laha 2015). Despite this, the remanence and coercivity are extremely near to zero (shown in the inset of Fig. 8), preventing the particle agglomeration and indicating improved dispersion in the solution.

These findings showed that self-assembled Fe<sub>3</sub>O<sub>4</sub> nanoparticles have very unique magnetic properties, such as large  $M_s$  and magnetic in the same sample, which is vast for self-assembled Fe<sub>3</sub>O<sub>4</sub> microparticles with large  $M_s$ , as opposed to conventional magnetic labels like magnetic polymer beads and nanoparticles (Xu et al. 2016). The microparticles are particularly

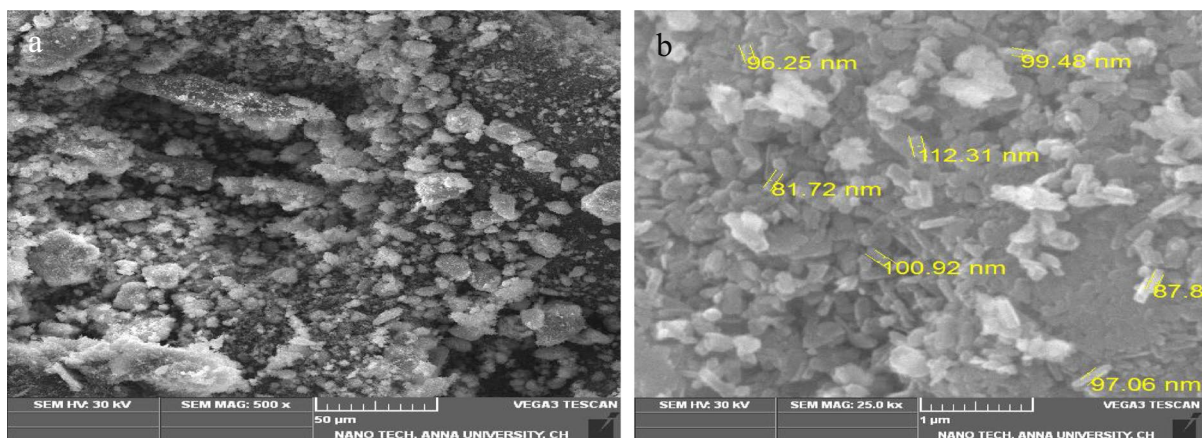


**Fig. 8** SEM image at 500 $\times$  (a) and 2500 $\times$  (b)

well suited for bio-detection as a magnetic label due to their decreased remanence and high dispersion in the solution. The hysteresis analysis of  $Fe_3O_4$  is shown in Fig. 9.

The variation of distance with sensor output for various input voltages is shown in Fig. 10. From Fig. 10, it is observed that when the distance between the sensor and biasing magnet increases, the voltage output of the sensor decreases. Hence, it is concluded that the field at the sensor is directly proportional to the distance between the sensor and biasing magnet.

The GMR sensor response using the test setup is shown in Fig. 11 and 12 whereas the sensor magnetic field changes from  $-2$  mT to  $2$  mT. The maximum sensor output was roughly  $275$  mV, which corresponds to a  $1.7$  mT applied magnetic field intensity

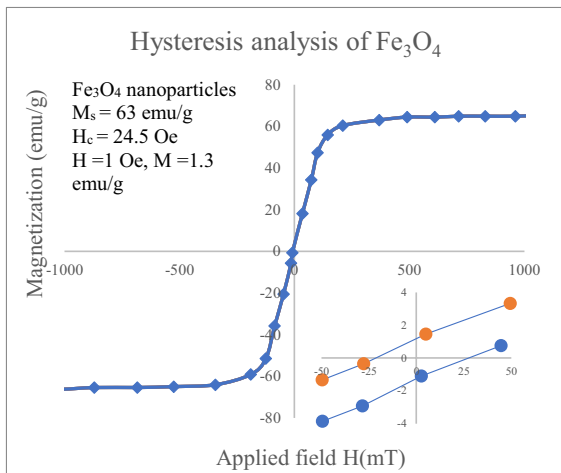


Fig. 9 Hysteresis analysis of  $Fe_3O_4$

Fig. 10 Distance vs Sensor output for various input voltages

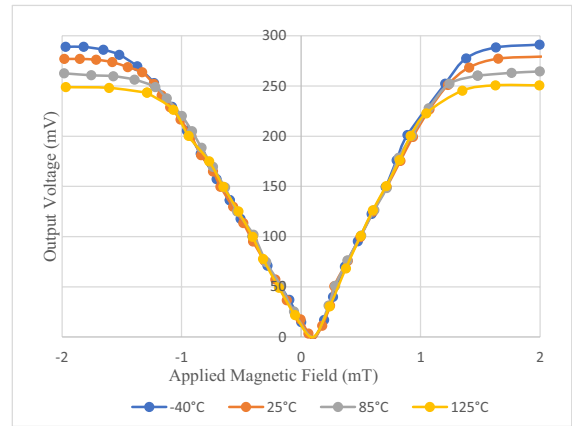
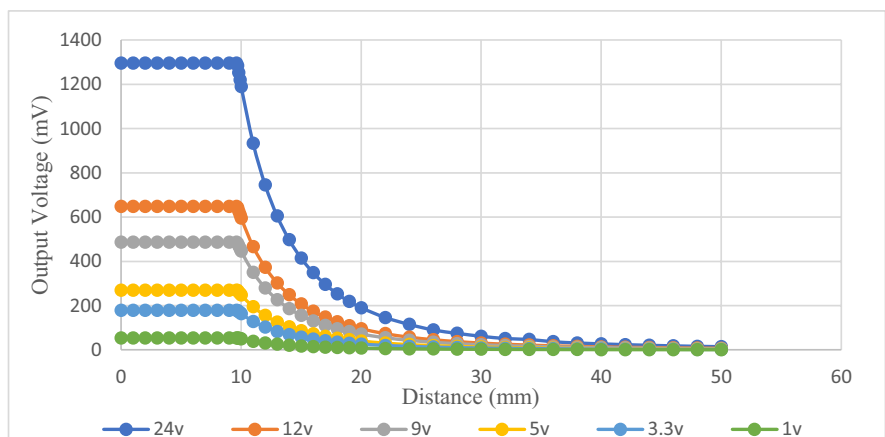
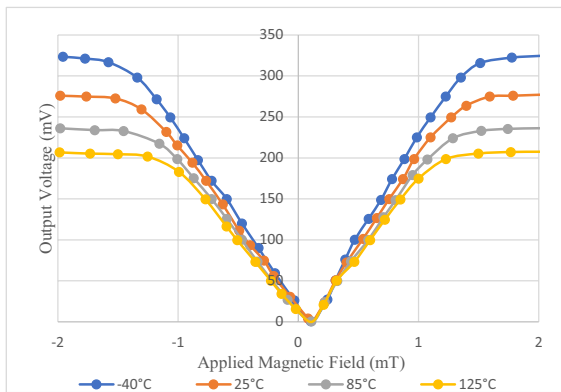


Fig. 11 AA002 Temperature performance, 5 V supply

in the air. There was typical hysteresis, with a linear range of roughly  $0.1$  mT to  $1.5$  mT. The sensor itself might be the source of sensor hysteresis. When the GMR sensor is utilized for magnetic particle quantification without sensor bias, the sensor output voltage would be at its lowest in the absence of a magnetic field (Park 2015).

Figure 11 and 12 illustrate the sensor’s increasing voltage response in both positive and negative magnetic field directions. Also, the GMR sensor response against the temperature change is linear. The sensor bias method increased the detection sensitivity of the GMR sensor for magnetic particle quantification. In the biased situation with permanent magnets, the hysteresis was substantially decreased.

Figure 13 shows the off-axis distance analysis of the sensor. It is important to identify the off-axis

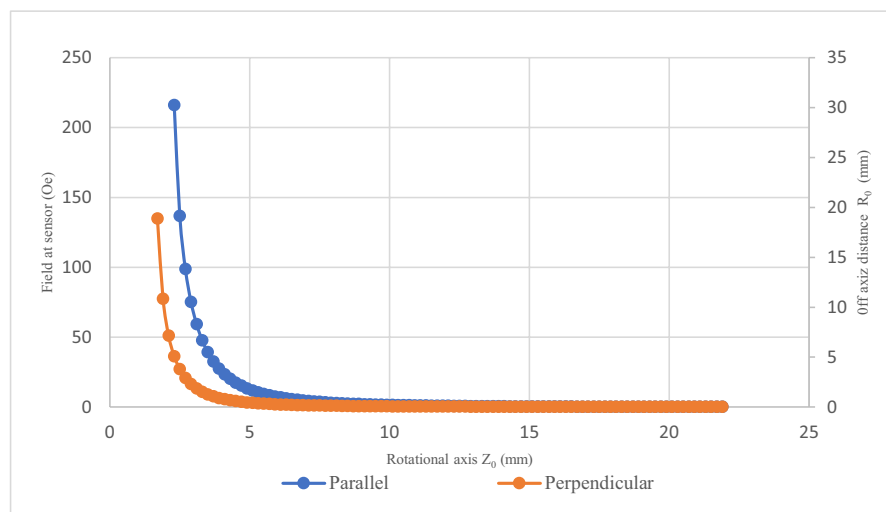


**Fig. 12** AA002 Temperature performance, 1 mA current supply

distance between the GMR sensor and the bias magnet. Figure 13 shows that the parallel and perpendicular off-axis distance analysis. Based on this parallel and perpendicular off-axis analysis, the optimal off-axis and rotational axis can be obtained for the sensor design. Parallel off-axis analysis provides better module arrangements.

The MNPs of varies concentration ranges from 0 to 1  $\mu\text{g}$ . The conventionally available Lutron Gauss meter was used to prepare and measure the stock precursor solution, further serial dilution is followed as mentioned in our previous research work (Anand et al. 2021). Initially, calibration was performed with known sample concentrations and the voltage output was obtained and with the reference to the readings, it is possible to detect the unknown sample

**Fig. 13** Off plane axis angle sensing

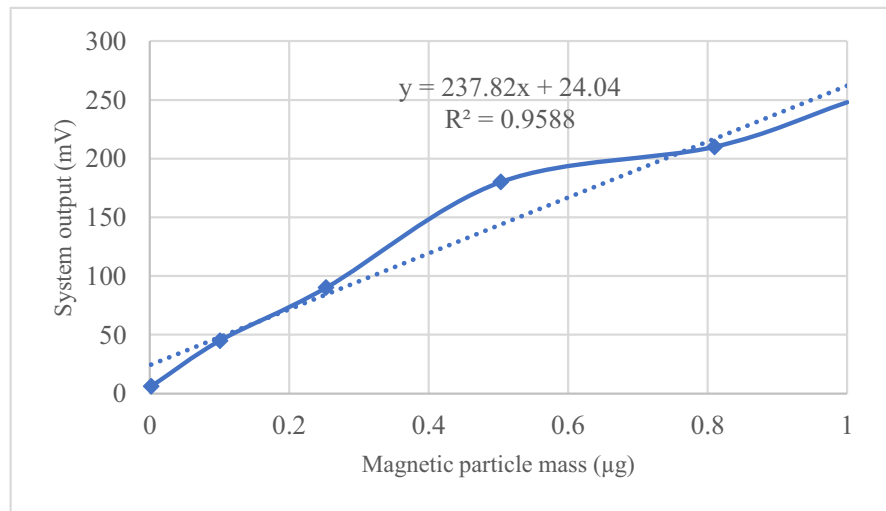


concentrations. The voltage values obtained at different concentrations were charted in Fig. 14. The detection limit is 36 ng.

## Conclusion

Based on the comparison of various single objective optimization techniques, the optimal magnetic biasing value has been identified and incorporated in the design. The detection limit was further reduced to detect the lowest magnetic nanoparticle concentration of 36.5 ng compared with the previously designed device detection limit of 43.5 ng (Park 2015). Variance-based sensitivity analysis is used to identify the most influencing parameter as magnetic bias. Using the single objective optimization technique, the magnetic biasing value has been optimized as  $H=35$  Oe. Also, various signal condition circuits have been analyzed for the design. Based on the quantitative analysis the final analog signal conditioning circuit has been incorporated into the design. Using RPT design, various blocks such as Magnetic holder, Sensor holder, Sample holder have been fabricated for the design. The off-axis analysis is performed to arrange the modules for better sensitivity. Scanning Electron Microscope technique was carried out to study the structure and size of the  $\text{Fe}_3\text{O}_4$  magnetic nanoparticle used for this analysis. The nanoparticles were magnetized and the GMR sensor was biased by the vertical and horizontal magnetic fields generated by the diagonally positioned neodymium magnets. The

**Fig. 14** Different concentration vs Output voltage



temperature analysis shows that the GMR sensor performance decreases when the temperature increases. This proposed design will be useful for the quantification of various bio-elements in real-time for various biomedical and environmental applications.

**Author contribution** Anand. G, Thyagarajan. T, Kokila K, Kamal C have equally contributed.

**Data availability** The datasets generated during the current study are available from the corresponding author on reasonable request.

#### Declarations

**Conflict of interest** The authors declare that they have no conflict of interest.

#### References

- Anand G, Thyagarajan T, Ramakrishnan S (2021) "Fluorescence nanoparticle detection in a liquid sample using the smartphone for biomedical application fluorescence nanoparticle detection in a liquid sample using the smartphone for biomedical application," *J Fluorescence*, pp. 0–8. <https://doi.org/10.1007/s10895-021-02799-w>
- Anand G, Thyagarajan T, Aashique Roshan B, Rajeshwar L, Shyam Balaji R (2022) Signal conditioning circuits for GMR sensor in biomedical applications. In: Subramani C, Vijayakumar K, Dakyo B, Dash SS (eds) *Proceedings of international conference on power electronics and renewable energy Systems. Lecture notes in electrical engineering*, vol 795. Springer, Singapore. [https://doi.org/10.1007/978-981-16-4943-1\\_10](https://doi.org/10.1007/978-981-16-4943-1_10)
- Atalay S, Kolat VS, Atalay FE, Bayri N, Kaya H, Izgi T (2018) Magnetoelastic sensor for magnetic nanoparticle

- detection. *J Magn Magn Mater* 465:151–155. <https://doi.org/10.1016/j.jmmm.2018.05.108>
- Behera B et al (2021) Design and development of GMR based low range pressure sensor for medical ventilator application. *Sensors Actuators, A Phys* 321:1–14. <https://doi.org/10.1016/j.sna.2021.112581>
- Bhaskarrao NK, Anoop CS, Dutta PK (2017) "A simple signal conditioner for tunneling magneto-resistance based angle sensor," *2016 IEEE Annu. India Conf. INDICON 2016*, pp. 1–6. <https://doi.org/10.1109/INDICON.2016.7839065>
- Chakkarapani K, Thangavelu T, Dharmalingam K, Thandavarayan P (2019) Multiobjective design optimization and analysis of magnetic flux distribution for slotless permanent magnet brushless DC motor using evolutionary algorithms. *J Magn Magn Mater* 476(2018):524–537. <https://doi.org/10.1016/j.jmmm.2019.01.029>
- Crespo RD, Elbaile L, Carrizo J, García JA (2018) Optimizing the sensitivity of a GMR sensor for superparamagnetic nanoparticles detection: micromagnetic simulation. *J Magn Magn Mater* 446:37–43. <https://doi.org/10.1016/j.jmmm.2017.08.066>
- Daughton JM (2000) GMR and SDT sensor applications. *IEEE Trans. Magn.* 36(5 I):2773–2778. <https://doi.org/10.1109/20.908586>
- Djamal M, Ramli R (2017) Giant magnetoresistance sensors based on ferrite material and its applications. Bandung
- Elangovan K, Anoop CS (2020) "A digital signal-conditioner for resistive sensors and its utility for linearizing GMR-based magnetometer," *2020 IEEE Sensors Appl. Symp. SAS 2020 - Proc.* <https://doi.org/10.1109/SAS48726.2020.9220031>.
- Laha SS (2015) "Understanding the physics of magnetic nanoparticles and their applications in the biomedical field," *ProQuest Diss. Theses*, p. 139, [Online]. Available: [http://search.proquest.com/docview/1728804023?accountid=14701%5Cnhttp://sfx.scholarsportal.info/ottawa?url\\_ver=Z39.88-2004&rft\\_val\\_fmt=info:ofi/fmt:kev:mtx:dissertation&genre=dissertations+%26+theses&sid=ProQ:ProQuest+Dissertations+%26+Theses+Global&atitl](http://search.proquest.com/docview/1728804023?accountid=14701%5Cnhttp://sfx.scholarsportal.info/ottawa?url_ver=Z39.88-2004&rft_val_fmt=info:ofi/fmt:kev:mtx:dissertation&genre=dissertations+%26+theses&sid=ProQ:ProQuest+Dissertations+%26+Theses+Global&atitl)

- Lee CP, Lai MF, Huang HT, Lin CW, Wei ZH (2014) Wheatstone bridge giant-magnetoresistance based cell counter. *Biosens Bioelectron* 57:48–53. <https://doi.org/10.1016/j.bios.2014.01.028>
- Li Y et al (2010) Nanomagnetic competition assay for low-abundance protein biomarker quantification in unprocessed human sera. *J Am Chem Soc* 132(12):4388–4392. <https://doi.org/10.1021/ja910406a>
- Li L, Mak KY, Leung CW, Ng SM, Lei ZQ, Pong PWT (2013) Detection of 10-nm superparamagnetic iron oxide nanoparticles using exchange-biased GMR sensors in wheatstone bridge. *IEEE Trans Magn* 49(7):4056–4059. <https://doi.org/10.1109/TMAG.2013.2237889>
- Manteca A, Mujika M, Arana S (2011) GMR sensors: magnetoresistive behaviour optimization for biological detection by means of superparamagnetic nanoparticles. *Biosens Bioelectron* 26(8):3705–3709. <https://doi.org/10.1016/j.bios.2011.02.013>
- Murzin D et al (2020) Ultrasensitive magnetic field sensors for biomedical applications. *Sensors (switzerland)* 20(6):1–32. <https://doi.org/10.3390/s20061569>
- Muşuroi C, Oproiu M, Volmer M, Neamtu J, Avram M, Helerea E (2021) Low field optimization of a non-contacting high-sensitivity gmr-based dc/ac current sensor. *Sensors* 21(7):1–20. <https://doi.org/10.3390/s21072564>
- Park J (2015) Superparamagnetic nanoparticle quantification using a giant magnetoresistive sensor and permanent magnets. *J Magn Magn Mater* 389:56–60. <https://doi.org/10.1016/j.jmmm.2015.04.049>
- Park J (2016) A giant magnetoresistive reader platform for quantitative lateral flow immunoassays. *Sensors Actuators A Phys* 250:55–59
- Reig C, Cubells-Beltrán MD, Muñoz DR (2009) Magnetic field sensors based on Giant Magnetoresistance (GMR) technology: Applications in electrical current sensing. *Sensors* 9(10):7919–7942. <https://doi.org/10.3390/s91007919>
- Smith CH, Schneider RW (1998) Magnetic field sensing utilizing GMR materials. *Sens Rev* 18(4):230–236. <https://doi.org/10.1108/02602289810240592>
- Sun Y, Fang L, Wan Y, Gu Z (2018) Pathogenic detection and phenotype using magnetic nanoparticle-urease nanosensor. *Sensors Actuators, B Chem* 259:428–432. <https://doi.org/10.1016/j.snb.2017.12.095>
- Xu J et al (2016) Detection of the concentration of MnFe<sub>2</sub>O<sub>4</sub> magnetic microparticles using giant magnetoresistance sensors. *IEEE Trans Magn* 52(4):10–13
- Zhang D, Pan Z, Zhou H, Zhang W (2016) Magnetic sensor based on giant magneto-impedance effect using the self-regulating technology on the bias magnetic field. *Sensors Actuators, A Phys* 249:225–230. <https://doi.org/10.1016/j.sna.2016.09.005>

**Publisher's note** Springer Nature remains neutral with regard to jurisdictional claims in published maps and institutional affiliations.

Springer Nature or its licensor holds exclusive rights to this article under a publishing agreement with the author(s) or other rightsholder(s); author self-archiving of the accepted manuscript version of this article is solely governed by the terms of such publishing agreement and applicable law.